Chinese Journal of
POLYMER SCIENCE

RESEARCH ARTICLE

• 2026 Rising Scholars •

https://doi.org/10.1007/s10118-026-3819-y
Chinese J. Polym. Sci.

Dendronized Hyperbranched Polymers with Excellent Second-order Nonlinear Performance through Topological Structure Modulation

Pan-Pan Qiao[a,†], Kai Wang[a,†], Wen-Tao Yuan[a], Qian-Qian Li[a*], and Zhen Li[a,b*]

[a] *Hubei Key Lab on Organic and Polymeric Opto-Electronic Materials, Department of Chemistry, Wuhan University, Wuhan 430072, China*
[b] *College of Chemistry and Chemical Engineering, Hubei University, Wuhan 430062, China*

Electronic Supplementary Information

Abstract The development of organic second-order nonlinear optical (NLO) materials critically depends on achieving a non-centrosymmetric arrangement of chromophores to maximize macroscopic NLO coefficients. Recently, dendronized hyperbranched polymers (DHPs) have emerged as promising candidates due to their unique spatial architectures, which suppress unfavorable aggregation and stabilize ordered orientation. The central cores serve as a key factor governing the branching topology of the resulting polymers. Herein, a series of DHPs were constructed by regulating the configuration of branching cores containing ether bonds with low rotational barriers. Driven by the synergy between an optimized static topological architecture and the dynamic modulation of low-rotational-barrier linkers, DHP-PhO achieved an optimal combination of a high NLO coefficient (d_{33}=263 pm·V^{-1}) and robust thermal stability ($T_{80\%}$=120 °C). This work provides a viable molecular design strategy for developing high-performance organic NLO polymers through the integration of topological engineering and core structure modulation, which is expected to promote the practical application of organic NLO materials in advanced optoelectronic devices.

Keywords Second-order nonlinear optical effect; Thermostability; Dendronized hyperbranched polymers; Topological modulation

Citation: Qiao, P. P.; Wang, K.; Yuan, W. T.; Li, Q. Q.; Li, Z. Dendronized hyperbranched polymers with excellent second-order nonlinear performance through topological structure modulation. *Chinese J. Polym. Sci.* https://doi.org/10.1007/s10118-026-3819-y

INTRODUCTION

Organic second-order nonlinear optical (NLO) materials have attracted attention due to their high microscopic NLO coefficients (β) of chromophores, ease of structural modification, low dielectric constant, and excellent processability, endowing them with unparalleled competitiveness in integrated photonic applications.[1–3] Generally, the macroscopic NLO coefficients (d_{33}) are primarily determined by the β values of the chromophores and their arrangement in a preferred non-centrosymmetric orientation. However, the strong dipole-dipole interactions among adjacent chromophore units tend to drive the formation of thermodynamically stable centrosymmetric aggregates.[4–8] Consequently, even when electric field poling is applied above the glass transition temperature of the polymers to induce a non-centrosymmetric orientation of the chromophores (Fig. 1a), the resulting d_{33} values remain limited due to imperfect chromophore alignment.[9,10]

Various strategies have been developed to regulate molecular orientation precisely.[11–14] Among them, the evolution of polymer topological architectures has opened a new route to enhancing NLO performance. Traditional linear polymers adopt random-coil conformations that severely restrict chromophore alignment, resulting in poor macroscopic polar order and weak electro-optic activity. In stark contrast, emerging topologies, such as cyclic, star-shaped, brush, and dendrimer-like polymers, pre-organize chromophores into spatially confined, orientationally ordered ensembles.[15–22] These architectures impose conformational constraints that enhance poling efficiency, stabilize the induced non-centrosymmetric alignment against thermal randomization, and suppress detrimental dipole-dipole interactions. By engineering the local microenvironment through chain topology, the desired molecular orientation can be effectively locked in. Integrating the complementary merits of dendritic and hyperbranched polymers (HPs), dendronized hyperbranched polymers (DHPs), innovatively proposed by our group in 2013, have now emerged as a novel and promising platform for constructing high-performance NLO materials.[23,24] The DHPs, generated by introducing low-generation dendrimers as monomers into the HPs backbone, feature novel spatial architectures, high degree of branching and facile synthesis. The spatial isolation effect induced by the three-dimensional structure of DHPs, coupled with their abundant cavity environments, facilitate the ordered arrangement of the chromophore moieties in the initial state. Therefore, these DHPs

* Corresponding authors, E-mail: liqianqian@whu.edu.cn (Q.Q.L.)
E-mail: lizhen@whu.edu.cn (Z.L.)
† These authors contributed equally to this work.
Received June 14, 2026; Accepted July 19, 2026; Published online September 4, 2026

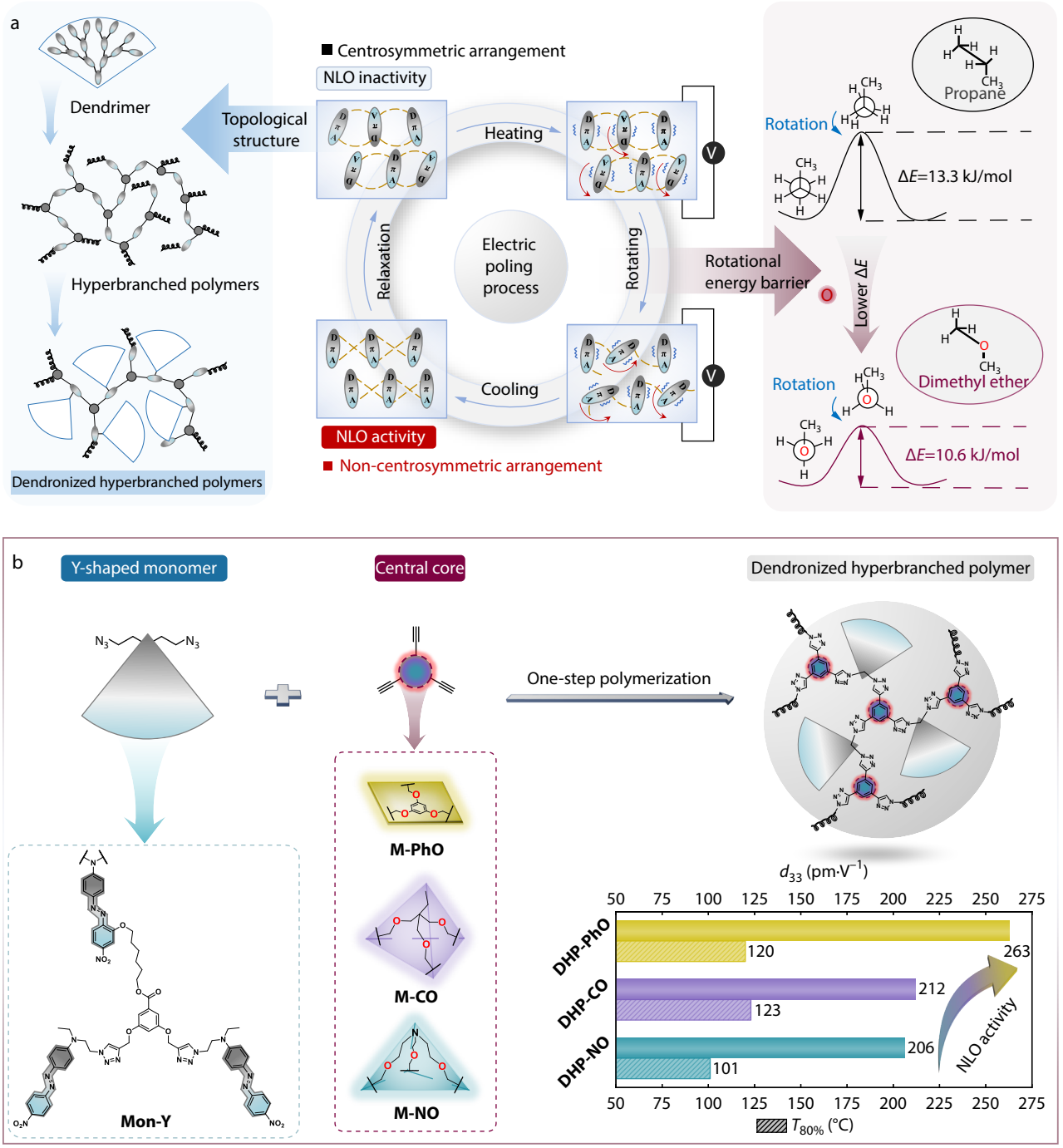

Fig. 1 (a) The non-centrosymmetric arrangement of chromophores achieved through the combination of external stimulus and structural regulation; (b) The synthesis and regulation of dendronized hyperbranched polymers *via* one-step polymerization, and the corresponding NLO performance.

exhibit superior NLO performance and enhanced thermal stability.[25–27]

Furthermore, to enhance the dynamic orientation of chromophore moieties during electric field poling process, our group investigated the often-overlooked linkers between chromophores and found that alkoxy chains markedly outperform conventional alkyl linkers.[28–31] This superiority originates from their intrinsically lower rotational energy barriers (ΔE), the ΔE value of dimethyl ether is only 10.6 kJ·mol^{-1} compared with 13.3 kJ·mol^{-1} of propane,[32,33] which allows chromophores to rotate more freely and align more efficiently during electric-field poling, leading directly to higher macroscopic polar order and improved poling efficiency. These findings establish linker chemistry not as a passive structural element, but as a critical and tunable molecular design parameter for optimizing chromophore orientation dynamics and boosting the electro-optic performance of NLO polymers.

Inspired by these findings, herein, we focused on core en-

gineering in DHPs incorporating preferred alkoxy chains. A series of DHPs was synthesized *via* one-step polymerization, in which Y-shaped monomers containing azo-chromophores served as the dendritic segments, and three types of comonomers incorporating ether bonds with low rotational energy barriers acted as the central cores (Fig. 1b). The distinct configurations of these three-dimensional branching points profoundly influence aggregation behavior of chromophores and ultimately the NLO properties. The optimized **DHP-PhO** achieved a large second-order NLO coefficient (d_{33}=263 pm·V^{-1}) and a thermal decay temperature ($T_{80\%}$= 120 °C). Our findings demonstrate that fine-tuning the topological structure and internal flexibility of DHPs by core engineering is an effective strategy for developing advanced organic second-order NLO materials.

EXPERIMENTAL

Materials

N,N-dimethylformamide (DMF) was dried and distilled from Na-K alloy under an atmosphere of dry nitrogen. All other reagents were used as received.

Instrumentation

The nuclear magnetic resonance (NMR) spectra (^{1}H- and ^{13}C-) were recorded on a Bruker AVANCE NEO (400 MHz for ^{1}H, 101 MHz for ^{13}C) spectrometer using tetramethylsilane (TMS; δ=0 ppm) as the internal standard. The matrix assisted laser desorption ionization time-of-flight mass spectra were measured with an AB SCIEX 5800 MALDI-TOF MS. The infrared (IR) absorption spectra were recorded with a PerkinElmer-2 spectrometer in the region of 4000–500 cm^{-1}. The gel permeation chromatography (GPC) analysis was performed using a Waters HPLC system equipped with a 2690D separation module and a 2410 refractive index detector. Polymethyl methacrylate (PMMA) was used as a calibration standard, and DMF was used as an eluent (25 °C and 1 mL·min^{-1}). The ultraviolet-visible (UV-Vis) absorption spectra were obtained using a Shimadzu UV-2700 spectrometer. The thermogravimetric analysis (TGA) was performed with a Beijing Hengjiu HTG-1 thermal analyzer at a heating rate of 10 °C·min^{-1} in nitrogen at a flow rate of 50 cm^3·min^{-1}. The differential scanning calorimetry (DSC) was performed using a Mettler-Toledo DSC3 under nitrogen at a scanning rate of 10 °C·min^{-1}. The thickness of the films was measured with a profiler (Bruker DEKTAKXT). Density functional theory (DFT) calculations were performed on Gaussian 16, Revision C01.[34] Molecular structure optimization was calculated based on PBE1PBE functional with DEF2SVP basis set. Visualization of intramolecular interactions was obtained through the Multiwfn 3.8 software.[35]

Synthesis of Dendronized Hyperbranched Polymers

Under an atmosphere of nitrogen, **M-NO**, **M-CO**, **M-PhO**, or **M-Ph** (1.00 equiv.) and **Mon-Y** (1.50 equiv.) were dissolved in DMF in a Schlenk flask at room temperature. A predetermined volume of freshly prepared aqueous copper (II) sulfate pentahydrate ($CuSO_4$·$5H_2O$, 0.08 mol·L^{-1}, about 0.10 equiv.) and aqueous sodium ascorbate (NaAsc, 0.16 mol·L^{-1}, about 0.10 equiv.) was then introduced *via* a microsyringe. After 24 h of reaction at room temperature, a second batch of aqueous solutions of $CuSO_4$·$5H_2O$ (about 0.05 equiv.) and NaAsc (about 0.05 equiv.) was added. The conversion of monomer **Mon-Y** was monitored by thin-layer chromatography (TLC), and the reaction was immediately quenched, once the monomer was mostly consumed but before insoluble product began to form. The mixture was poured into a large excess of water, and the resultant precipitate was collected and washed successively with deionized water, anhydrous methanol, and acetone. The crude product was further purified by reprecipitation from dichloromethane into methanol, yielding a deep-red powder.

*Synthesis of **DHP-NO***

Mon-Y (138.7 mg, 0.100 mmol), **M-NO** (17.7 mg, 0.067 mmol), DMF (10.0 mL), $CuSO_4$·$5H_2O$ aqueous solution (125 μL + 50 μL), NaAsc aqueous solution (125 μL + 50 μL), a deep red powder (121.0 mg, 77%). ^{1}H-NMR (400 MHz, DMSO-d_6, 298 K), δ (TMS, ppm): 8.30–8.20 (ArH), 7.86–7.70 (ArH), 7.08 (ArH), 6.93 (ArH), 6.76–6.71 (ArH), 5.14 (CH_2), 4.59 (CH_2), 4.40 (CH_2), 4.19 (CH_2), 3.86 (CH_2), 3.72 (CH_2), 3.58(CH_2), 3.19 (CH_2), 1.78–1.68 (CH_2), 1.45 (CH_2), 0.95 (CH_3).

*Synthesis of **DHP-CO***

Mon-Y (138.7 mg, 0.100 mmol), **M-CO** (16.6 mg, 0.067 mmol), DMF (10 mL), $CuSO_4$·$5H_2O$ aqueous solution (125 μL + 50 μL), NaAsc aqueous solution (125 μL + 50 μL), a deep red powder (130.0 mg, 84%). ^{1}H-NMR (400 MHz, DMSO-d_6, 298 K), δ (TMS, ppm): 8.28–8.20 (ArH), 7.85–7.69 (ArH), 7.10 (ArH), 6.88 (ArH), 6.75–6.70 (ArH), 5.15 (CH_2), 4.59 (CH_2), 4.40 (CH_2), 4.20 (CH_2), 3.86 (CH_2), 3.69 (CH_2), 3.57 (CH_2), 3.17 (CH_2), 1.80–1.70 (CH_2), 1.43 (CH_2), 0.95 (CH_3).

*Synthesis of **DHP-PhO***

Mon-Y (138.7 mg, 0.100 mmol), **M-PhO** (16.0 mg, 0.067 mmol), DMF (10 mL), $CuSO_4$·$5H_2O$ aqueous solution (125 μL + 50 μL), NaAsc aqueous solution (125 μL + 50 μL), a deep red powder (120.0 mg, 78%). ^{1}H-NMR (400 MHz, DMSO-d_6, 298 K), δ (TMS, ppm): 8.33–8.24 (ArH), 7.88–7.74 (ArH), 7.12 (ArH), 6.94 (ArH), 6.81–6.74 (ArH), 5.20 (CH_2), 4.64 (CH_2), 4.25 (CH_2), 3.93 (CH_2), 3.75 (CH_2), 3.63 (CH_2), 3.25 (CH_2), 1.84 (CH_2), 1.74 (CH_2), 1.51 (CH_2), 1.00 (CH_3).

*Synthesis of **DHP-Ph***

Mon-Y (138.7 mg, 0.100 mmol), **M-Ph** (10.0 mg, 0.067 mmol), DMF (10 mL), $CuSO_4$·$5H_2O$ aqueous solution (125 μL + 50 μL), NaAsc aqueous solution (125 μL + 50 μL), a deep red powder (73.0 mg, 49%). ^{1}H-NMR (400 MHz, DMSO-d_6, 298 K), δ (TMS, ppm): 8.38–8.21 (ArH), 7.94–7.72 (ArH), 7.11 (ArH), 7.01 (ArH), 6.83–6.71 (ArH), 5.20 (CH_2), 4.64 (CH_2), 4.28–4.22 (CH_2), 3.95–3.91 (CH_2), 3.74 (CH_2), 3.62 (CH_2), 3.23 (CH_2), 1.88 (CH_2), 1.75 (CH_2), 1.54 (CH_2), 0.95 (CH_3).

Film Preparation

The DHPs were dissolved in dichloromethane at a concentration of 30 mg·mL^{-1}. The solutions were thoroughly shaken and allowed to stand overnight to ensure complete swelling and dissolution of the polymers. Subsequently, the solutions were filtered through syringe filters (0.22 μm) and spin-coated onto the non-conductive side of indium-tin-oxide (ITO)-coated glass substrates. The purchased ITO-coated glass substrates (2.0 cm × 1.9 cm) were sequentially cleaned by ultrasonic treatment in different solvents: water, acetone, deionized water, DMF, and tetrahydrofuran (THF) prior to use. The transparent polymer films were prepared by spin-coating 75 μL of the polymer solution onto the substrate at two consecutive speeds: 1000 r·min^{-1} for 18 s and 1500 r·min^{-1} for 60 s, without intermediate delay.

Residual solvent was removed in a vacuum oven at 40 °C for 12 h. The resultant films typically possessed thicknesses of 100–200 nm (Table S1 in the electronic supplementary information, ESI), and showed good uniformity (Fig. S1 in ESI).

NLO Measurement

The second-order NLO efficiencies were measured *via in situ* second harmonic generation (SHG) experiments using a closed temperature-controlled oven equipped with optical windows and three needle electrodes, and were characterized by the d_{33} value as the SHG coefficient.[36,37] The films were kept at 45° to the incident beam, and the conductive plane faced the laser. The gap distance between this conductive plane and the needle electrodes is 8 mm. Then the laser was lit, the films were poled inside the oven at a poling voltage of 7.0 kV, and the SHG intensity was monitored simultaneously. The SHG measurements were carried out using an Nd: YAG laser operating at a 10 Hz repetition rate and an 8 ns pulse width at 1064 nm. A Y-cut quartz crystal served as the reference. The thin films were slowly heated from room temperature to the best poling temperature under an electric field. The de-poling curves of second-order NLO materials after poling were conducted as follows: poled films were heated gradually from room temperature until no obvious signals were observed in the absence of an applied electric field. The heating rate was 4 °C·min^{-1}.

RESULTS AND DISCUSSION

Synthesis and Characterization

The target DHPs were synthesized *via* the Click reaction between Y-shaped monomer and central cores (detailed synthesis see Scheme S1 in ESI), which features high synthetic yields (77%–84%).[38,39] Nevertheless, the polymerization procedure requires precise regulation to prevent excessive crosslinking, which would otherwise render the resultant products insoluble and infusible. Referring to the previous polymerization protocol established in our laboratory, a large amount of insoluble substances rapidly emerged in the reaction system under a monomer concentration of 0.01 mmol·mL^{-1} and a catalyst dosage of 0.20 equiv. Accordingly, the catalyst loading was reduced to 0.10 equiv. in the subsequent trial. An additional portion of catalyst (*ca.* 0.05 equiv.) was supplemented after 24 h of reaction, and the polymerization progress was monitored in real time. Specifically, a small amount of reaction solution was periodically dropped into methanol to observe precipitate formation and evaluate the solubility of the precipitated product. Once obvious precipitate appeared, water was immediately introduced to quench the reaction, so as to obtain polymers with high molecular weight as well as satisfactory solubility. The final products DHPs were all soluble in common polar organic solvents, such as CH_2Cl_2, DMF and dimethyl sulfoxide (DMSO). Variation in central core structures led to different optimal reaction durations for the obtained polymers. The central core **M-Ph** possesses high structural rigidity and poor solubility, thus corresponding to the shortest reaction time; insoluble fractions could be detected only 3 h after the second catalyst addition. In contrast, the introduction of ether linkages in **M-PhO** endowed it with better solubility, which prolonged the polymerization process. As a result, insoluble precipitates were observed until 16 h after the supplementary addition of the catalyst. Generally, unterminated hyperbranched polymers tend to undergo further crosslinking during storage, which inevitably impairs their solubility and processability. In comparison, the as-prepared polymers exhibit excellent storage stability. This favorable property is attributed to their unique spatial configuration, which effectively isolates individual chromophore units and generates considerable steric hindrance. This steric effect efficiently suppresses further crosslinking reactions.

The chemical structures of central cores and the resultant DHPs were initially characterized by ^{1}H- and ^{13}C-NMR spectra (Figs. S3–S13 in ESI). Fourier-transform infrared (FTIR) spectroscopy was further employed to identify functional groups and monitor the polymerization process (Fig. 2a). Notably, the characteristic peak at 2098 cm^{-1}, attributed to the azide group (—N_3), disappeared in the prepared polymers compared to the corresponding monomer **Mon-Y**, confirming the consumption of azide moieties *via* their reaction with alkynyl groups. The sustained presence of nitro-based chromophores throughout the polymerization was evidenced by the persistent bands at 1516 and 1335 cm^{-1}.

Thermal properties of the polymers were investigated by DSC and TGA. The thermal decomposition temperature (T_d, temperature at 5% weight loss) and glass transition temperature (T_g) are summarized in Table 1. **DHP-PhO** (T_g=122 °C) showed the highest T_g value, higher than those of **DHP-NO** (T_g=93 °C), **DHP-CO** (T_g=114 °C), and **DHP-Ph** (T_g=119 °C) (Fig. 2b). All polymers exhibit high T_d above 250 °C, attributed to the excellent thermal stability of the azo-chromophores (Fig. 2c). The molecular weights of target polymers were determined by GPC. All four dendronized hyperbranched polymers possess weight-average molecular weight (M_w) higher

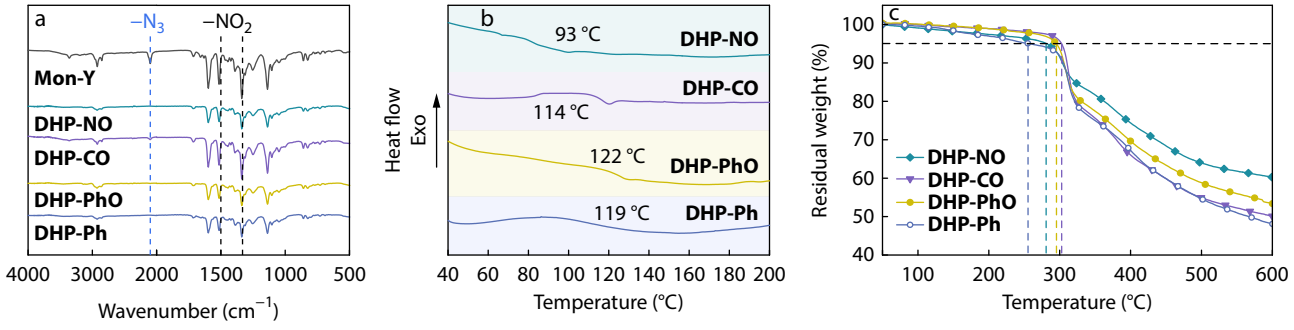

Fig. 2 (a) FTIR spectra of target polymers and the corresponding monomer **Mon-Y**; (b) DSC curves and (c) TGA thermograms of polymers measured at a heating rate of 10 °C·min^{-1} under nitrogen atmosphere.

than 10^4, with a lower polydispersity index (Table 1).

Chromophores with strong intramolecular charge transfer (ICT) effect, demonstrated solvent-dependent absorption spectra. The absorption spectra of the monomer and polymers were measured in six kinds of solvents (Fig. S2 in ESI), and the corresponding maximum absorption wavelengths were listed in Table S2 (in ESI). The corresponding maximum absorption wavelengths red-shifted gradually with the increased polarity of solvents from 1,4-dioxane to DMSO. The difference between its maximum absorption wavelength in 1,4-dioxane and that in DMSO was defined as $\Delta\lambda_{max}$. Although the same chromophore (The molecule features a diazene (—N=N—) core bridging two phenyl rings, with an electron-donating unit [—$N(CH_3)_2$] and an electron-withdrawing nitro group (—NO_2) at the para-position, respectively.) in this system, the $\Delta\lambda_{max}$ values of DHPs (29–32 nm), were slightly smaller than that of monomer **Mon-Y** (35 nm). The free **Mon-Y** chromophore underwent enhanced electron delocalization when exposed to the highly polar media. In contrast, the three-dimensional hyperbranched framework of DHPs acts as a physical barrier for the embedded chromophores. This spatial confinement creates a distinct local environment compared to the free monomer, effectively shielding the chromophores from the influence of polar solvents. Consequently, while both the free **Mon-Y** chromophore and the chromophores embedded in the DHP frameworks exhibit solvatochromism, the interaction between the chromophores in DHPs and the external solvent is attenuated.

Second-order NLO Properties

The second-order NLO responses of DHPs were investigated *via in situ* second harmonic generation (SHG) measurements, with the SHG coefficient d_{33} and thermal decay temperature $T_{80\%}$ employed as key parameters to evaluate NLO activity and temporal stability. The method for the calculation of the d_{33} for the poled films has been reported previously. The poling curves of the SHG coefficients of polymer films as a function of temperature are shown in Fig. 3(a). All four DHPs exhibited excellent

Table 1 Characterization data and NLO properties of polymer.

Polymer	M_w [a] (10^4)	M_w/M_n [a] (PDI)	T_g [b] (°C)	T_d [c] (°C)	λ_{max} [d] (nm)	l_s [e] (nm)	T_e [f] (°C)	d_{33} [g] (pm·V^{-1})	$d_{33(\infty)}$ [h] (pm·V^{-1})	$T_{80\%}$ [i] (°C)	Φ [j]	N [k] (%)
DHP-NO	3.09	1.44	93	281	468	158	120	206	38	101	0.34	53.7
DHP-CO	3.47	1.56	114	302	466	170	122	212	40	123	0.35	54.2
DHP-PhO	2.86	1.96	122	295	470	127	133	263	46	120	0.38	54.4
DHP-Ph	2.08	2.66	119	259	470	119	135	248	44	116	0.37	57.6

[a] Determined by GPC in DMF based on calibration with PMMA (25 °C and 1 mL·min^{-1}); [b] Glass transition temperature detected by DSC analysis under nitrogen at a heating rate of 10 °C·min^{-1}; [c] The 5% weight loss temperature of polymers detected by TGA analysis under nitrogen at a heating rate of 10 °C·min^{-1}; [d] The maximum absorption wavelength of polymer films; [e] Film thickness; [f] The best poling temperature corresponding to the highest SHG signal; [g] SHG coefficients measured at a 1064 nm fundamental beam at a voltage of 7 kV, representing the second-order NLO effect; [h] The non-resonant d_{33} values were calculated using an approximate two-level model, representing the NLO effect after deducting the fundamental frequency optical resonance; [i] The temperature at which the SHG signal decreased to 80%; [j] Order parameter for characterizing the orientation arrangement of chromophores, $\Phi = 1–A_1/A_0$, where A_1 and A_0 are the absorbance values of the polymer film after and before corona poling, respectively; [k] The loading density of the effective chromophores.

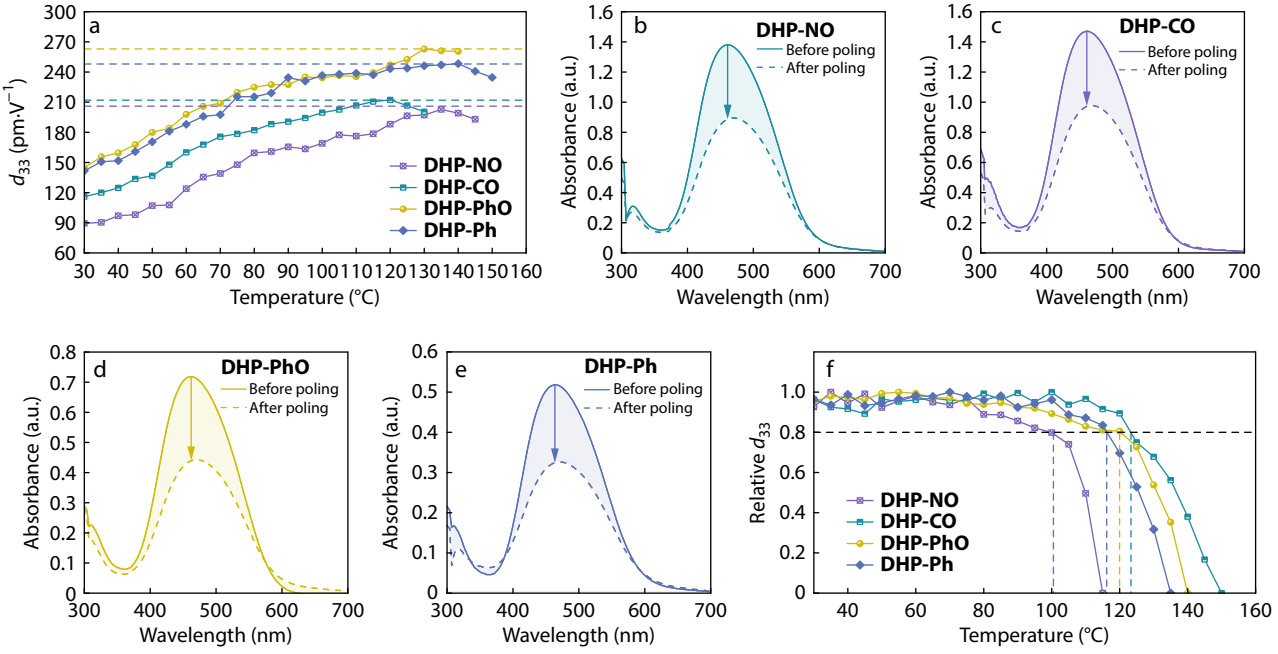

Fig. 3 (a) Poling curves of the SHG coefficient (d_{33}) of polymer films as a function of temperature; UV-Vis spectra of polymer films (b) **DHP-NO**, (c) **DHP-CO**, (d) **DHP-PhO** and (e) **DHP-Ph** before (solid) and after poling (dashed); (f) Decay curves of the SHG coefficient (d_{33}) of polymer films as a function of temperature.

https://doi.org/10.1007/s10118-026-3819-y

macroscopic NLO coefficients, with d_{33} values exceeding 200 pm·V^{-1}. It mainly benefited from the unique structural merits of dendronized hyperbranched architectures. The three-dimensional hyperbranched frameworks provide abundant free volume cavities, which effectively isolate chromophore units and weaken intermolecular dipole-dipole interactions. Meanwhile, the incorporation of ether bonds, which possess low rotational energy barriers, into the central cores facilitates chromophore rotation owing to the decreased energy barriers. Additionally, the head-to-tail linkage of Y-shaped chromophore monomers offer pre-optimized alignment at the molecular level. All of them promote the non-centrosymmetric alignment of chromophores during poling, elevating the NLO performance of DHPs in this system.

Moreover, the spatial configuration of the cores significantly influenced NLO performance (Table 1): the d_{33} values increased from 206 pm·V^{-1} (**DHP-NO**) to 212 pm·V^{-1} (**DHP-CO**), and further to 248 pm·V^{-1} (**DHP-Ph**) and 263 pm·V^{-1} (**DHP-PhO**) as the core configuration changes, with the order parameters (Φ) exhibited a corresponding increase from 0.34 to 0.35 and ultimately to 0.37 and 0.38 (Figs. 3b–3e). The $d_{33(\infty)}$ values (defined as the macroscopic NLO coefficients of non-resonance enhancement) of polymers were calculated using an approximate two-level model. To a certain extent, the $d_{33(\infty)}$ values can represent the NLO effect after deducting the fundamental frequency optical resonance, which demonstrated a similar trend to that of d_{33} values. Systematic investigations into the configuration of central core demonstrated that superior NLO performance in polymers correlated with a higher degree of planarity of central core. Fig. 4(a) displayed the optimized conformations of three types of simplified central cores obtained through theoretical calculations. **M-NO** and **M-CO** adopted similar trigonal pyramidal configurations, which forced the branched chains to grow unidirectionally. Consequently, **DHP-NO** and **DHP-CO** tend to form asymmetric hyperbranched topologies, that deviate from the ideal spherical structure recommended by the site isolation principle, thereby yielding lower d_{33} values.

In contrast, **M-PhO** exhibited a planar symmetric configuration, in which three branches were uniformly distributed and spatially well separated, thereby facilitating tri-directional extension of the branched chains. Such a regular hyperbranched topology optimized the alignment of chromophores to the greatest extent, and endowed **DHP-PhO** with the highest d_{33} value. To further distinguish the effect of the planar core topology and the dynamic flexibility of ether linkages, a control polymer **DHP-Ph**, lacking ether linkages on the benzene ring was prepared. Consistent with expectations, **DHP-Ph** demonstrated a high d_{33} value of 248 pm·V^{-1}. Specifically, **DHP-Ph** outperformed **DHP-NO** (d_{33}=206 pm·V^{-1}) and **DHP-CO** (d_{33}=212 pm·V^{-1}), confirming that a planar core served as an effective approach for topological optimization. In contrast, **DHP-Ph** exhibits a slightly lower d_{33} value than that of **DHP-PhO** (263 pm·V^{-1}), implying that the topological structure of the central core played a dominant role in enhancing NLO performance; the ether linkages provided a necessary dynamic boost for the chromophore alignment during the poling process. The high NLO coefficients were achieved through synergistic optimization of static topological architecture and dynamic modulation.

In the de-poling process of these polymers, the real-time decays of their SHG signals were monitored with the temperature ranging from 30 °C to 150 °C in the air at the rate of 4 °C·min^{-1} (Fig. 3f). The $T_{80\%}$ values (defined as the temperature at which the SHG signals decreased to an initial 80%) are 101 °C for **DHP-NO**, 123 °C for **DHP-CO**, 120 °C for **DHP-PhO**, and

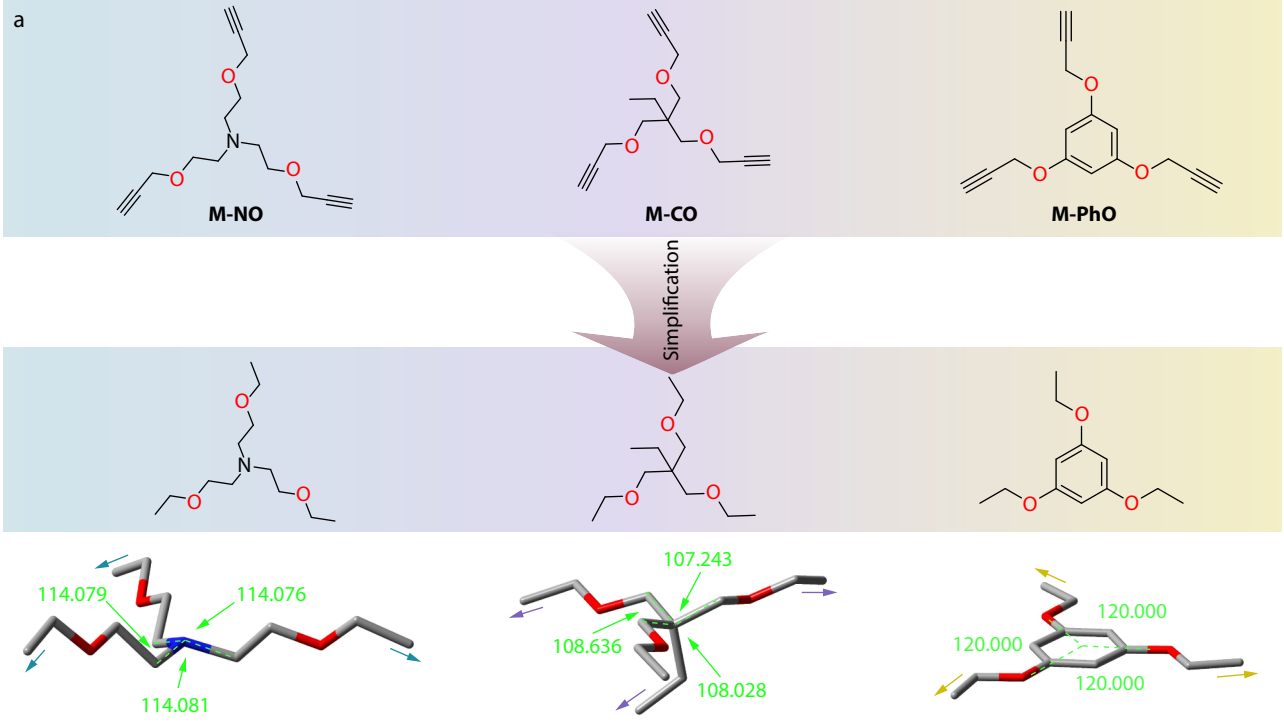

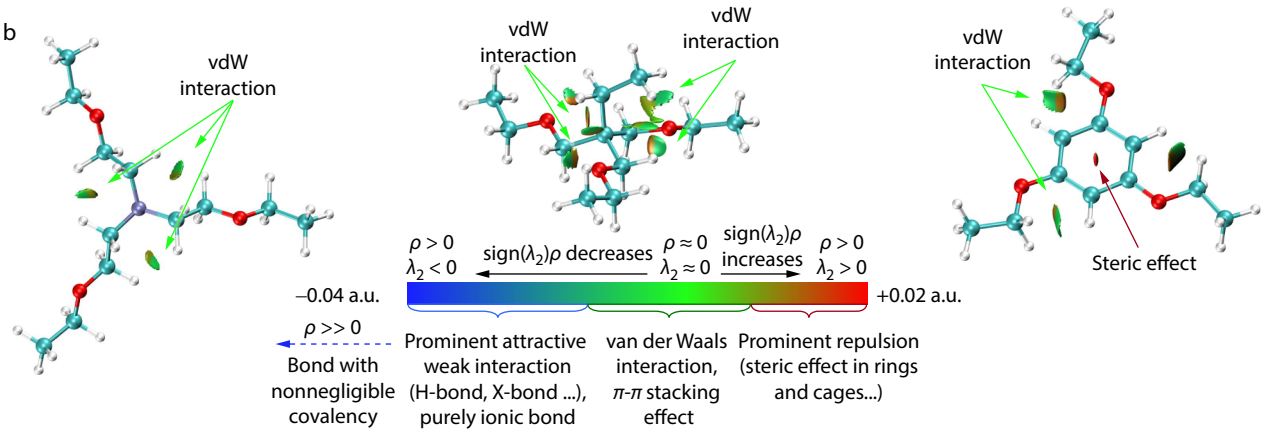

Fig. 4 (a) Molecular conformations of simplified central cores optimized by Gaussian 16, Revision C01 based on PBE1PBE functional with DEF2SVP basis set; (b) Visualization of intramolecular interactions of simplified central cores was obtained through the Multiwfn 3.8 software. The noncovalent interaction (NCI) maps of representative systems highlight noncovalent interactions. The simplified **M-NO** and **M-CO** primarily depict vdW interactions (green). The simplified **M-PhO** illustrates vdW interactions (green) and steric effects (red). The color bar indicates the sign(λ_2)ρ values, with blue representing prominent attractive interactions, red indicating prominent repulsive interactions in the regions with steric effect, and green exhibiting weak interactions, where ρ is the electron density, λ_2 is the second-largest eigenvalue of the electron density Hessian matrix.

116 °C for **DHP-Ph**. **DHP-PhO** and **DHP-Ph** benefit from the rigid planar benzene cores, which restrict chain motion and suppress chromophore relaxation. The flexible core of **DHP-NO** accelerated thermal relaxation of oriented chromophores after poling, resulting in poor thermal stability. Although **DHP-CO** shared a similar branching topology with **DHP-NO**, the ethyl group in **M-CO** produced relatively stronger, intensive intramolecular interactions with the other three branched chains, as visualized by noncovalent interaction (NCI) analysis (Fig. 4b)[40]. These interactions act as physical constraints to lock chromophore alignment, leading to exceptional thermal stability comparable with **DHP-PhO**. From this perspective, apart from topological considerations, augmenting intramolecular interactions, especially those governed by core regulation, represented another critical approach to improving the optical stability of polymers. Among all polymers, **DHP-PhO** achieved the optimal combination of large d_{33} (263 pm·V^{-1}) and high $T_{80\%}$ (120 °C), which significantly outperforms previously reported hyperbranched or dendronized hyperbranched NLO polymers with azo-chromophore moieties (Table S3 in ESI).[16,23,26–27,41–52] The promising topological design strategy with the rational modulation of molecular arrangements can be extended to other optoelectronic materials, which were also sensitive to aggregated structures.[53–60]

CONCLUSIONS

In summary, this work introduces a concise topology-regulation strategy for second-order NLO polymers by engineering central core configurations. Three key roles of the central core in boosting NLO performance are identified: core modification tailored the three-dimensional branched architecture of DHPs, supplying sufficient free volume for chromophore isolation and rotation; ether linkages with low rotational energy barriers assisted dynamic chromophore orientation under electric fields, ensuring high poling efficiency; and intramolecular interactions within the core enhanced the stability of the macroscopic optical response. Accordingly, **DHP-PhO** with a planar symmetric core achieved a d_{33} of 263 pm·V^{-1} and a thermal stability of 120 °C. The one-pot synthesis, good solubility, and excellent electro-optic parameters render these polymers promising for integrated photonic devices. This core-design concept is extendable to various branched electro-optic materials.

BIOGRAPHY

2026 Rising Scholar: Qian-Qian Li received her B.Sc. degree from Hubei University in 2004 and her Ph.D. degree from Wuhan University in 2009. She is currently a full professor at Wuhan University, where her research focuses on the modulation of aggregated structures in optoelectronic functional materials. She has published over 100 papers in journals, including *Angew. Chem. Int. Ed.*, *Adv. Mater.*, *Sci. Adv.*, *Nat. Commun.*, and *Light Sci. Appl.*, *etc.* Her publications have received over 12000 citations, with an H-index of 66.

Conflict of Interests

Zhen Li is an editorial board member for *Chinese Journal of Polymer Science* and was not involved in the editorial review or the decision to publish this article. The authors declare no interest conflict.

Electronic Supplementary Information

Electronic supplementary information (ESI) is available free of charge in the online version of this article at http://doi.org/10.1007/s10118-026-3819-y.

Data Availability Statement

The data supporting the findings of this study are available from the corresponding author upon reasonable request. Author's

contact information: liqianqian@whu.edu.cn, lizhen@whu.edu.cn.

ACKNOWLEDGMENTS

This work was financially supported by the National Natural Science Foundation of China (Nos. 22235006 and 22475157), the Foundation of Hubei Scientific Committee (Nos. 2024AFA021 and 2024BAB014). We are grateful to National Supercomputing Center in Shenzhen and Beijing Parallel Technology Corporation for theoretical calculation support.

REFERENCES

1 Marder, S. R.; Kippelen, B.; Jen, A. K. Y.; Peyghambarian, N. Design and synthesis of chromophores and polymers for electro-optic and photorefractive applications. *Nature* **1997**, *388*, 845–851.
2 Steier, W. H.; Chen, A.; Lee, S. S.; Garner, S.; Zhang, H.; Chuyanov, V.; Dalton, L. R.; Wang, F.; Ren, A. S.; Zhang, C.; Todorova, G.; Harper, A.; Fetterman, H. R.; Chen, D.; Udupa, A.; Bhattacharya, D.; Tsap, B. Polymer electro-optic devices for integrated optics. *Chem. Phys.* **1999**, *245*, 487–506.
3 Dalton, L. R.; Sullivan, P. A.; Bale, D. H. Electric field poled organic electro-optic materials: state of the art and future prospects. *Chem. Rev.* **2010**, *110*, 25–55.
4 Liao, Q. Y.; Li, Q. Q.; Li, Z. The key role of molecular packing in luminescence property: from adjacent molecules to molecular aggregates. *Adv. Mater.* **2025**, *37*, 2306617.
5 Tang, S. Y.; Wu, H. R.; Gu, J. Q.; Yuan, W. T.; Li, Q. Q.; Li, Z. Endowing photodeformation film with near-infrared afterglow. *Aggregate* **2025**, *6*, e70221.
6 Gao, Y.; Yuan, W. T.; Li, Y. X.; Huang, A. R.; Fang, Y. Y.; Li, A. S.; Wang, K.; Zou, B.; Li, Q. Q.; Li, Z. Accurately adjusted phenothiazine conformations: reversible conformation transformation at room temperature and self-recoverable stimuli-responsive phosphorescence. *Light Sci. Appl.* **2025**, *14*, 99.
7 Gao, Y.; Lu, J.; Liao, Q. Y.; Li, S. H.; Li, Q. Q.; Li, Z. Thermal annealing promoted room temperature phosphorescence: motion models and internal mechanism. *Natl. Sci. Rev.* **2023**, *10*, nwad239.
8 Wang, J. Q.; Li, Z.; Li, Q. Q. Organic high-temperature afterglow materials: an advancing and impactful research area. *Sci. China Mater.* **2025**, *68*, 406–412.
9 Huang, A. R.; Li, Q. Q.; Li, Z. Molecular uniting set identified characteristic (MUSIC) of organic optoelectronic material. *Chin. J. Chem.* **2022**, *40*, 2356–2370.
10 Li, Q. Q.; Li, Z. Molecular packing: another key point for the performance of organic and polymeric optoelectronic materials. *Acc. Chem. Res.* **2020**, *53*, 962–973.

Graphical Abstract

Dendronized Hyperbranched Polymers with Excellent Second-order Nonlinear Performance through Topological Structure Modulation

Pan-Pan Qiao, Kai Wang, Wen-Tao Yuan, Qian-Qian Li, and Zhen Li

Wuhan University; Hubei University

Dendronized hyperbranched polymers with regulated central cores achieved enhanced second-order nonlinear optical coefficients and robust thermal stability through synergistic optimization of static topological architecture and dynamic modulation of low-rotational-barrier linkers.

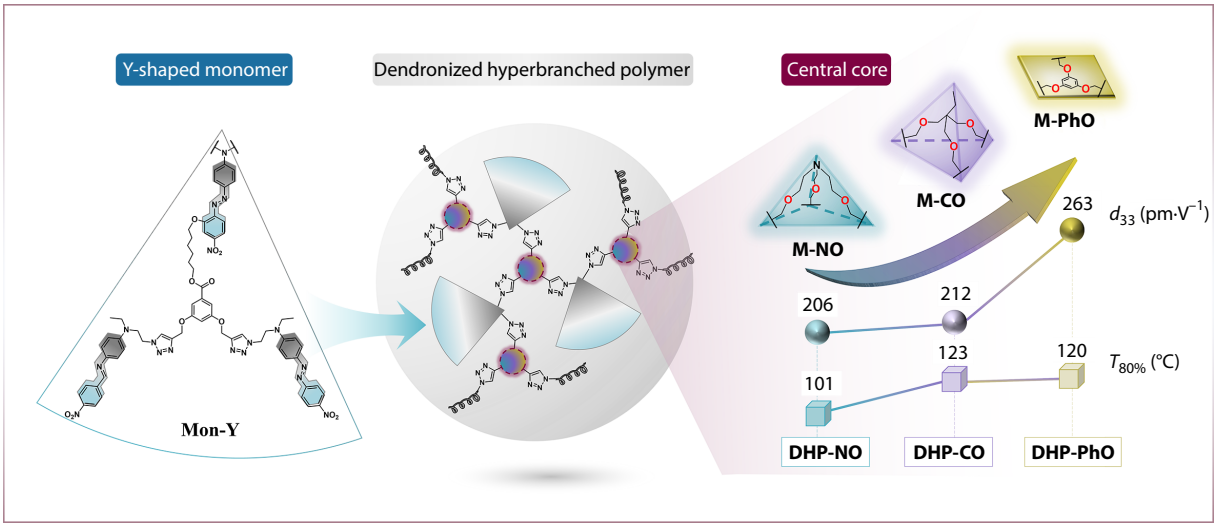

Chinese J. Polym. Sci. 2026 *https://doi.org/10.1007/s10118-026-3819-y*

11 Kim, T. D.; Kang, J. W.; Luo, J.; Jang, S. H.; Ka, J. W.; Tucker, N.; Benedict, J. B.; Dalton, L. R.; Gray, T.; Overney, R. M.; Park, D. H.; Herman, W. N.; Jen, A. K. Y. Ultralarge and thermally stable electro-optic activities from supramolecular self-assembled molecular glasses. *J. Am. Chem. Soc.* **2007**, *129*, 488–489.
12 Shi, Z.; Luo, J.; Huang, S.; Zhou, X. H.; Kim, T. D.; Cheng, Y. J.; Polishak, B. M.; Younkin, T. R.; Block, B. A.; Jen, A. K. Y. Reinforced site isolation leading to remarkable thermal stability and high electrooptic activities in cross-linked nonlinear optical dendrimers. *Chem. Mater.* **2008**, *20*, 6372–6377.
13 Li, Z.; Li, Q. Q.; Qin, J. G. Some new design strategies for second-order nonlinear optical polymers and dendrimers. *Polym. Chem.* **2011**, *2*, 2723–2740.
14 Qiao, P. P.; Li, Q. Q.; Li, Z. Optimization strategies for comprehensive performance of organic second-order nonlinear optical materials. *Chin. Sci. Bull.* **2023**, *68*, 4015–4034.
15 Li, Z. A.; Yu, G.; Liu, Y. Q.; Ye, C.; Qin, J. G.; Li, Z. Dendronized polyfluorenes with high azo-chromophore loading density: convenient synthesis and enhanced second-order nonlinear optical effects. *Macromolecules* **2009**, *42*, 6463–6472.
16 Wu, W. B.; Wang, C.; Zhong, C.; Ye, C.; Qiu, G. F.; Qin, J. G.; Li, Z. Changing the shape of chromophores from "H-type" to "star-type": increasing the macroscopic NLO effects by a large degree. *Polym. Chem.* **2013**, *4*, 378–386.
17 Wu, W. B.; Tang, R.; Li, Q. Q.; Li, Z. Functional hyperbranched polymers with advanced optical, electrical and magnetic properties. *Chem. Soc. Rev.* **2015**, *44*, 3997–4022.
18 Chen, P. Y.; Li, Z. The design of second-order nonlinear optical dendrimers: From "branch only" to "root containing". *Chinese J. Polym. Sci.* **2017**, *35*, 793–798.
19 Li, H.; Xue, Z. J.; Xue, Y. H.; Li, Y. X.; Liu, H. Topological structure evolution of polymer network based on star-shaped multi-armed precursors. *Chinese J. Polym. Sci.* **2025**, *43*, 1240–1252.
20 Liao, Q. Friction between strongly compressed polymer brushes. *Chinese J. Polym. Sci.* **2024**, *42*, 1368–1374.
21 Tian, N.; Li, Y. Q.; Gan, H. Y.; Ning, Z. B.; Jiang, N.; Gan, Z. H. Synergistic effect of multi-arm architecture and molecular weight on crystallization and degradation behavior of star-shaped poly(lactic acid). *Chinese J. Polym. Sci.* **2024**, *42*, 1948–1956.
22 Tu, F. Y.; Wang, M. F.; Zhong, G.; Qiao, H. W.; Zheng, B. T.; Liu, C. P.; Chen, M. F.; Zhang, H. G. One-step preparation of brush-type polystyrene (PS)-SiO_2-poly(2-hydroxyethyl methacrylate) janus nanoparticle to compatibilize PS/poly(methyl methacrylate) blends. *Chinese J. Polym. Sci.* **2025**, *43*, 1375–1386.
23 Wu, W. B.; Huang, L. J.; Fu, Y. J.; Ye, C.; Qin, J. G.; Li, Z. Design, synthesis and nonlinear optical properties of "dendronized hyperbranched polymers". *Chin. Sci. Bull.* **2013**, *58*, 2753–2761.
24 Tang, R. L.; Li, Z. Second-order nonlinear optical dendrimers and dendronized hyperbranched polymers. *Chem. Rec.* **2017**, *17*, 71–89.
25 Tang, R. L.; Chen, H.; Zhou, S. M.; Liu, B. W.; Gao, D.; Zeng, H. Y.; Li, Z. The integration of an "X" type dendron into polymers to further improve the comprehensive NLO performance. *Polym. Chem.* **2015**, *6*, 6680–6688.
26 Wu, W. B.; Xu, Z.; Li, Z. Using low generation dendrimers as monomers to construct dendronized hyperbranched polymers with high nonlinear optical performance. *J. Mater. Chem. C* **2014**, *2*, 8122–8130.
27 Wu, W. B.; Wang, Z. Y.; Xiao, R.; Xu, Z.; Li, Z. Main chain dendronized hyperbranched polymers: convenient synthesis and good second-order nonlinear optical performance. *Polym. Chem.* **2015**, *6*, 4396–4403.
28 Wang, K.; Deng, X. C.; Li, Q. Q.; Li, Z. Promotion of the second-order nonlinear optical effect by introducing ether linkage into polymer main chains. *Polym. Chem.* **2023**, *14*, 2205–2211.
29 Qiao, P. P.; Yuan, W. T.; Li, Q. Q.; Li, Z. High second-order nonlinear optical effect achieved by gradually decreased rotational energy barriers. *Polym. Chem.* **2025**, *16*, 441–449.
30 Qiao, P. P.; Li, Q. Q.; Li, Z. Photo-crosslinked second-order nonlinear optical polymer films with large nonlinear optical effect and high thermostability. *Chinese J. Polym. Sci.* **2026**, *44*, 1007–1016.
31 Qiao, P. P.; Li, Q. Q.; Li, Z. Second-order nonlinear optical polymers with large NLO effect and high thermostability. *Macromol. Chem. Phys.* **2025**, *226*, e00082.
32 Buono, R. A.; Zauhar, R. J.; Venanzi, C. A. Ab initio rotational barriers and solvation free energies of fluorinated dimethyl ethers. *J. Mol. Struct.* **1996**, *370*, 97–133.
33 Sabbaghian, E.; Mehdipour-Ataei, S.; Jalilian, S.; Esfahanizadeh, M.; Salehi, A. M.; Khodabakhshi, F.; Jalalian, E. Novel species of soluble thermally stable poly(keto ether Ether amide)s: preparation, characterization, and properties. *Polym. Adv. Technol.* **2015**, *26*, 1–9.
34 Frisch, M. J.; Trucks, G. W.; Schlegel, H. B.; Scuseria, G. E.; Robb, M. A.; Cheeseman, J. R.; Scalmani, G.; Barone, V.; Petersson, G. A.; Nakatsuji, H.; Li, X.; Caricato, M.; Marenich, A. V.; Bloino, J.; Janesko, B. G.; Gomperts, R.; Mennucci, B.; Hratchian, H. P.; Ortiz, J. V.; Izmaylov, A. F.; Sonnenberg, J. L.; Williams; Ding, F.; Lipparini, F.; Egidi, F.; Goings, J.; Peng, B.; Petrone, A.; Henderson, T.; Ranasinghe, D.; Zakrzewski, V. G.; Gao, J.; Rega, N.; Zheng, G.; Liang, W.; Hada, M.; Ehara, M.; Toyota, K.; Fukuda, R.; Hasegawa, J.; Ishida, M.; Nakajima, T.; Honda, Y.; Kitao, O.; Nakai, H.; Vreven, T.; Throssell, K.; Montgomery Jr., J. A.; Peralta, J. E.; Ogliaro, F.; Bearpark, M. J.; Heyd, J. J.; Brothers, E. N.; Kudin, K. N.; Staroverov, V. N.; Keith, T. A.; Kobayashi, R.; Normand, J.; Raghavachari, K.; Rendell, A. P.; Burant, J. C.; Iyengar, S. S.; Tomasi, J.; Cossi, M.; Millam, J. M.; Klene, M.; Adamo, C.; Cammi, R.; Ochterski, J. W.; Martin, R. L.; Morokuma, K.; Farkas, O.; Foresman, J. B.; Fox, D. J. *Gaussian 16 Rev. B.01*, Wallingford, CT, 2016.
35 Lu, T.; Chen, F. W. Multiwfn: A multifunctional wavefunction analyzer. *J. Comput. Chem.* **2012**, *33*, 580–592.
36 Singer, K. D.; Sohn, J. E.; Lalama, S. J. Second harmonic generation in poled polymer films. *Appl. Phys. Lett.* **1986**, *49*, 248–250.
37 Sugihara, O.; Nakayama, H.; Okamoto, N.; Sakakibara, T.; Taketani, Y. Nonlinear optical properties of poled polymer of phenoxy resin containing α-cyano unsaturated carboxylate. *Jpn. J. Appl. Phys.* **1994**, *33*, L321.
38 Rostovtsev, V. V.; Green, L. G.; Fokin, V. V.; Sharpless, K. B. A Stepwise huisgen cycloaddition process: copper(I)-catalyzed regioselective "ligation" of azides and terminal alkynes. *Angew. Chem. Int. Ed.* **2002**, *41*, 2596–2599.
39 Kolb, H. C.; Finn, M. G.; Sharpless, K. B. Click chemistry: diverse chemical function from a few good reactions. *Angew. Chem. Int. Ed.* **2001**, *40*, 2004–2021.
40 Lu, T. Visualization analysis of covalent and noncovalent interactions in real space. *Angew. Chem. Int. Ed.* **2025**, *64*, e202504895.
41 Li, Z. A.; Wu, W. B.; Ye, C.; Qin, J. G.; Li, Z. New second-order nonlinear optical polymers derived from AB_2 and AB monomers via snogashira coupling reaction. *Macromol. Chem. Phys.* **2010**, *211*, 916–923.
42 Li, Z. A.; Yu, G.; Hu, P.; Ye, C.; Liu, Y. Q.; Qin, J. G.; Li, Z. New azo-chromophore-containing hyperbranched polytriazoles derived from AB_2 monomers via click chemistry under copper(I) catalysis. *Macromolecules* **2009**, *42*, 1589–1596.
43 Wu, W. B.; Li, Z. Further improvement of the macroscopic NLO coefficient and optical transparency of hyperbranched polymers by enhancing the degree of branching. *Polym. Chem.* **2014**, *5*, 5100–5108.

https://doi.org/10.1007/s10118-026-3819-y

44 Wu, W. B.; Ye, C.; Qin, J. G.; Li, Z. The utilization of isolation chromophore in an "A_3+B_2" type second-order nonlinear optical hyperbranched polymer. *Macromol. Rapid Commun.* **2013**, *34*, 1072–1079.

45 Wu, W. B.; Huang, L. J.; Xiao, L.; Huang, Q.; Tang, R. L.; Ye, C.; Qin, J. G.; Li, Z. New second-order nonlinear optical (NLO) hyperbranched polymers containing isolation chromophore moieties derived from one-pot "A_2 + B_4" approach via Suzuki coupling reaction. *RSC Adv.* **2012**, *2*, 6520–6526.

46 Wu, W. B.; Ye, C.; Yu, G.; Liu, Y. Q.; Qin, J. G.; Li, Z. New hyperbranched polytriazoles containing isolation chromophore moieties derived from AB_4 monomers through Click chemistry under copper(I) catalysis: improved optical transparency and enhanced NLO effects. *Chem. Eur. J.* **2012**, *18*, 4426–4434.

47 Li, Z. A.; Wu, W. B.; Ye, C.; Qin, J. G.; Li, Z. New main-chain hyperbranched polymers: Facile synthesis, structural control, and second-order nonlinear optical properties. *Polymer* **2012**, *53*, 153–160.

48 Wu, W. B.; Fu, Y. J.; Wang, C.; Ye, C.; Qin, J. G.; Li, Z. A series of hyperbranched polytriazoles containing perfluoroaromatic rings from AB_2-type monomers: convenient syntheses by click chemistry under copper(I) catalysis and enhanced optical nonlinearity. *Chem. Asian J.* **2011**, *6*, 2787–2795.

49 Zang, X. B.; Liu, G. C.; Li, Q. Q.; Li, Z. A.; Li, Z. A correlation study between dendritic structure and macroscopic nonlinearity for second-order nonlinear optical materials. *Macromolecules* **2020**, *53*, 4012–4021.

50 Yang, H. T.; Tang, R. L.; Wu, W. B.; Liu, W.; Guo, Q.; Liu, Y. L.; Xu, S. G.; Cao, S. K.; Li, Z. A series of dendronized hyperbranched polymers with dendritic chromophore moieties in the periphery: convenient synthesis and large nonlinear optical effects. *Polym. Chem.* **2016**, *7*, 4016–4024.

51 Wu, W. B.; Xiao, R.; Xiang, W. D.; Wang, Z. P.; Li, Z. Main chain dendronized polymers: design, synthesis, and application in the second-order nonlinear optical (NLO) area. *J. Phys. Chem. C* **2015**, *119*, 14281–14287.

52 Tang, R. L.; Chen, H.; Zhou, S. M.; Xiang, W. D.; Tang, X.; Liu, B. W.; Dong, Y. Q.; Zeng, H. Y.; Li, Z. Dendronized hyperbranched polymers containing isolation chromophores: design, synthesis and further enhancement of the comprehensive NLO performance. *Polym. Chem.* **2015**, *6*, 5580–5589.

53 Yu, J. N.; Zhou, J. M.; Wang, Z.; Chen, R. F.; Feng, X. X.; Zhang, Y.; Wu, N.; Xin, S. Flame-retardant quasi-solid polymer electrolytes for building stable and dendrite-free lithium metal batteries. *Sci. China Chem.* **2026**, *69*, 698–702.

54 Chen, Y. T.; Jiang, C. Z.; Liu, S. W.; Yuan, W. T.; Li, Q. Q.; Li, Z. Promoting photocatalytic hydrogen evolution by stabilization of excited triplet states and enhancement of internal electric field at dye/PCN interface. *Angew. Chem. Int. Ed.* **2025**, *64*, e202419850.

55 Wang, M.; Liu, X. X.; Yuan, W. T.; Yang, Y. J.; Zhong, C.; Wu, B. X.; Li, Z.; Li, Q. Q. Building a highly stable red/near infrared afterglow library with highly branched structures. *Adv. Mater.* **2025**, *37*, 2415446.

56 Wang, J. Q.; Yang, Y. J.; Zhang, L. Y.; Li, Z. Engineering organic photochromism with photoactivated phosphorescence: multifunctional smart devices and enhanced four-channel data storage. *Adv. Mater.* **2025**, *37*, 2503074.

57 Gong, Y. X.; Zhang, W. C.; Liu, Z. J.; Fang, M. M.; Yang, J.; Wang, Y. S.; Gao, M. X.; Zhang, J.; Yang, Q. H.; Li, Z. Phenothiazine derivatives as small-molecule organic cathodes with adjustable dropout voltage and cycle performance. *Adv. Mater.* **2024**, *36*, 2312486.

58 Li, J.; Gu, J.; Ding, L.; Li, X.; Xia, P.; Liu, F.; Chen, X.; Ma, W.; He, Y.; Li, Q.; Li, Z.; Yuan, Y. Near-infrared organic room temperature phosphorescent probes targeting fibroblast activation protein for surgical navigation of liver cancer. *Aggregate* **2025**, *6*, e70031.

59 Ma, X.; Ye, T.; Yang, H.; Ling, G.; Wang, D.; Li, J.; Gu, P.; Xu, L.; Sheng, T.; Lin, F.; Shen, R.; Zhang, Q. Dynamic color-tunable ultra-long room temperature phosphorescence polymers with photochromism and water-stimuli response for multilevel anti-counterfeiting. *Aggregate* **2024**, *5*, e579.

60 Shan, Y.; Sheng, J.; Zhang, Q.; Stuart, M. C. A.; Qu, D.; Feringa, B. L. Multi-state photoluminescent properties of an overcrowded alkene-based molecular motor in aggregates. *Aggregate* **2024**, *5*, e584.